

Spectral variations of light scattering by marine particles in coastal waters, from visible to near infrared

David Doxaran,^{a,*} Kevin Ruddick,^b David McKee,^c Bernard Gentili,^a Dominique Tailliez,^a Malik Chami,^a and Marcel Babin^a

^a Université Pierre et Marie Curie, Laboratoire d’Océanographie de Villefranche, Centre National de la Recherche Scientifique, Villefranche-sur-Mer, France

^b Royal Belgian Institute of Natural Sciences, Management Unit of the North Sea Mathematical Models, Brussels, Belgium

^c Department of Physics, University of Strathclyde, Glasgow, United Kingdom

Abstract

Field measurements and Mie calculations of the particulate light-scattering coefficient (b_p , in m^{-1}) in the near-infrared and visible spectral domains are combined to quantify and model the effect of particulate absorption on the b_p spectral variations. The case of particles of coastal origin and assumed to follow a Junge-type size distribution is considered. A simple power-law function closely reproduces the near-infrared b_p spectral variations, with a spectral slope varying in the range 0.1–1.4. In the visible (e.g., 440 nm), particulate absorption effects systematically lead to b_p values 5–30% lower than values predicted using a power-law function fitted in the near infrared and extrapolated to 440 nm. The respective influences of the particle size distribution and composition are investigated for both mineral and organic particle populations. Finally, an empirical model derived from theoretical calculations closely reproduces the actual b_p spectral variations from near-infrared to short visible wavelengths, taking into account particulate absorption effects.

The propagation of solar radiation in natural waters is controlled by light absorption and scattering by pure seawater and the different colored dissolved and particulate substances contained in the water. These substances are often grouped within three main categories: phytoplankton, nonalgal particles, and colored dissolved organic matter. In coastal waters, light scattering by suspended particles strongly affects light propagation in the water column (Lee et al. 2005), and determines to a large extent the magnitude of surface reflectance (Sathyendranath et al. 1989). This is especially true in the near infrared (near IR) where, to a first approximation and consistently with the observations of Doxaran et al. (2002) and Ruddick et al. (2006), the water reflectance depends only upon three inherent optical properties: the pure seawater absorption coefficient and the backscattering coefficient of pure seawater and suspended particles. Therefore, assuming realistic values of the particle-scattering coefficient turns out to be essential when modeling light propagation in coastal waters, possibly to estimate primary production, when interpreting surface reflectance in terms of optically significant seawater constituents (Doerffer and Schiller 2007), and when trying to separate the ocean and atmospheric contributions from the reflectance signal detected at the top of atmosphere (Moore et al. 1999).

On the basis of simple theoretical considerations, Morel (1973) showed that a polydispersion of nonabsorbing particles with a homogenous index of refraction and a size distribution that follows an inverse power law is characterized by spectral variations of its scattering coefficient that also follow an inverse power-law function. This simple spectral dependency of $b_p(\lambda)$, sometimes extended to the

backscattering coefficient $b_{bp}(\lambda)$, has been often used in models of the inherent optical properties of seawater (Sathyendranath et al. 1989; Roesler and Perry 1995; Morel and Maritorena 2001), mostly because no sound alternative is available. Doxaran et al. (2007) recently confirmed on the basis of observations made in a number of estuaries that, in the near-IR spectral region where light absorption by marine particles is low (Babin and Stramski 2002), a power-law function does fit the spectral variations of $b_p(\lambda)$ with variable slope. Such a power-law function, however, is inappropriate in the visible part of the spectrum where marine particles are light absorbing: particulate light absorption increases approximately exponentially toward short visible wavelengths in the case of mineral and detrital particles and presents more complex variations generally with two maxima in the blue and in the red in the case of phytoplankton cells. Numerous measurements of $b_p(\lambda)$ spectra have documented significant departures from a power-law function at wave bands associated with strong particulate absorption (Barnard et al. 1998; Babin et al. 2003a; Stramski et al. 2007). Particulate absorption influences the particulate scattering properties in a complicated way (Bricaud and Morel 1986; Morel and Bricaud 1986), so that there is currently no model to realistically reproduce the $b_p(\lambda)$ spectral variations in the visible region. Boss et al. (2001b) assumed that spectral variations of the particulate attenuation coefficient ($c_p[\lambda] = b_p[\lambda] + a_p[\lambda]$, with a_p the particulate absorption coefficient) can be represented as a power-law function. This implies that the departure of $b_p(\lambda)$ from a smooth power-law function is simply compensated by the particulate absorption coefficient, $a_p(\lambda)$, which is not valid according to the Mie theory (Morel and Bricaud 1981) but may be appropriate in practice (Boss et al. 2001b). But Doxaran et al. (2007)

* Corresponding author: doxaran@obs-vlfr.fr

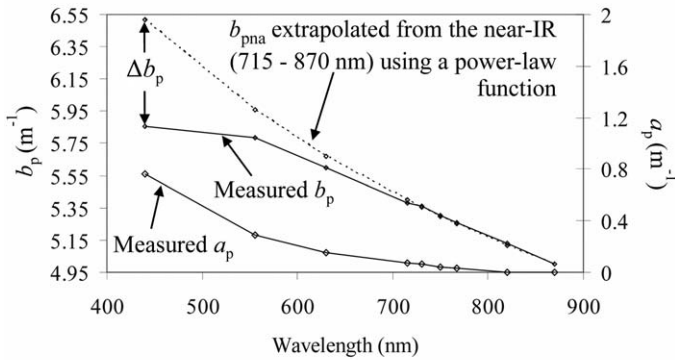


Fig. 1. Typical spectral differences between measured b_p values and modeled b_{pna} values obtained by extrapolation from the near-IR (715–870 nm) spectral region using the $b_p(870)\left(\frac{\lambda}{870}\right)^{-\gamma}$ power-law function (γ is the near-IR b_p spectral slope). The a_p and b_p spectra were measured in the Gironde estuary (France) in 2006.

found the spectral slope of $b_p(\lambda)$ in the near IR and that of $c_p(\lambda)$ in the visible to be significantly different, which suggests that the decrease of $b_p(\lambda)$ in the visible, due to particulate absorption effects, is not simply equal to $a_p(\lambda)$.

In this study, we examine how light absorption by particles affects the shape of the $b_p(\lambda)$ spectrum. The difference observed between the spectral variations of $b_p(\lambda)$ in the near-IR and visible regions is used as a reference for the departure of $b_p(\lambda)$ from a power-law function (see Fig. 1 for illustration). We first apply Mie theory to quantify the absorption effects as a function of the complex refractive index of particles and of the particle size distribution, under simplifying assumptions. From these simulations, an empirical model is developed to produce realistic $b_p(\lambda)$ spectra from the visible to the near-IR ranges that accounts for particle absorption and size. This new b_p spectral model is then validated using in situ $a_p(\lambda)$ and $b_p(\lambda)$ data collected in several European estuaries and coastal waters.

Theoretical background

Light scattering by a single particle depends on its geometrical cross-section (thus shape and size) and on its refractive index relative to that of the surrounding medium (seawater). The refractive index of particles relative to water can be written as:

$$m = n - in' \quad (1)$$

where n and n' are respectively the real and imaginary parts of the refractive index. Typical n values vary from 1.03 and a theoretical upper limit of 1.158 for organic particles (Morel and Ahn 1990; Aas 1996), depending on hydration, and from 1.07 to 1.22 for various minerals (Lide 2001). Woźniak and Stramski (2004) observed general tendency of increasing n with increasing density of minerals. Typical values and spectral variations for n' have been documented by Patterson et al. (1977), Egan and Higelman (1979), and Stramski et al. (2007).

In estuaries and coastal waters directly influenced by river inputs, single-grain mineral particles may either appear as individual particles in water or as aggregates containing water and organic matter. Large estuarine aggregates reaching sizes up to 1000 μm have been observed using video cameras (Kranck 1984). When considering a population of particles, their concentration (number of particles per unit volume of water sample containing these particles) and size are taken into account through the particle size distribution (PSD) (Jonasz and Fournier 2007). Different functions can be used to fit actual PSDs, such as exponential, log-normal, phi-normal, or hyperbolic distributions. In natural waters, the size distribution of suspended particles is often assumed to follow a simple power-law function, also called Junge size distribution (Bader 1970):

$$N(D) = KD^{-j} \quad (2)$$

where N is the number of particles of diameter D per cubic meter and per micrometer, K sets the concentration of particles, and j , often called Junge exponent, is the slope of the distribution. This exponent varies around a mean value of 4 and typically from 2.5 to 5 (Jonasz and Fournier 2007). For a fixed number of particles, the proportion of small particles increases when the exponent j increases. The use of Junge distributions for marine particles has been criticized (Risovic 2002; Stavn and Keen 2004; Chami et al. 2006). Although some field measurements carried out in coastal waters suggest PSDs close to a power-law distribution (Boss et al. 2001a), others reveal significant features at any size range on top of a power-law PSD (Bale and Morris 1987; Eisma et al. 1991; Bernard et al. 2001). Note also that current particle-sizing techniques for discrete and in situ sampling, such as the resistive particle-counting technique (e.g., Coulter counter) or laser diffraction (e.g., the LISST series, Sequoia Scientific), are typically limited to the range 1–200 μm (Agrawal and Pottsmith 2000). Apart for a few measurements reported by Stramski and Woźniak (2005) (see their figs. 1, 2), there is currently a lack of information concerning the finest fraction of particles ($<1 \mu\text{m}$) which, especially when it is mineral, contributes significantly to light scattering (see fig. 4a in Babin et al. 2003a).

Mie theory can be used to compute the optical properties of particles that are assumed homogeneous and spherical. Mie computations notably provide the efficiency factors for scattering and absorption (Q_b and Q_a). The corresponding coefficients are then obtained by integration over the size distribution:

$$b_p(\lambda) = \left(\frac{\pi}{4}\right) \int_{D_{\min}}^{D_{\max}} N(D) Q_b(\lambda, D, m) D^2 dD \quad (3)$$

$$a_p(\lambda) = \left(\frac{\pi}{4}\right) \int_{D_{\min}}^{D_{\max}} N(D) Q_a(\lambda, D, m) D^2 dD \quad (3')$$

where λ is the wavelength of light, whereas the minimum and maximum diameters, D_{\min} and D_{\max} , define the size interval. Theoretically, the spectral variations of b_p , in the case of nonabsorbing and homogeneous particles distrib-

uted in size according to Eq. 2 with D_{\min} and D_{\max} respectively equal to 0 and infinity, can be written:

$$b_p(\lambda) = A\lambda^{-\gamma} \quad (4)$$

The exponent of this power law, γ , also called scattering spectral slope, is then simply related to the slope of the PSD, j , through (Morel 1973):

$$\gamma = j - 3 \quad (5)$$

To verify Eq. 5 with the Mie theory, the actual limits D_{\min} and D_{\max} chosen for calculations in Eq. 3 must be small and large enough, respectively, to account for most of particle scattering at all wavelengths (Morel 1973; Boss et al. 2001b). This condition also applies to $a_p(\lambda)$ calculations for the sake of obtaining results independent of D_{\min} and D_{\max} .

Equations 4 and 5 are no longer valid in the case of absorbing particles ($n' > 0$). To understand the influence of particulate absorption on $b_p(\lambda)$, the effect of n' variations both on the real and imaginary parts of m must be considered. The former phenomenon can be explained and modeled according to the Ketteler–Helmholtz theory of anomalous dispersion (Bricaud and Morel 1986). It is significant in the vicinity of absorption bands such as the major ones observed on phytoplankton cells in the blue and red parts of the spectrum. In the case of detrital and mineral marine particles for which the absorption coefficient generally varies smoothly with wavelength, variations in n resulting from anomalous dispersion are negligible. The effect of absorption on $b_p(\lambda)$ through the contribution of n' to m , which is certainly much more important than the effect of anomalous dispersion even for phytoplankton, is accounted for by the Mie theory and expressed in the computed efficiency factors (Morel and Bricaud 1986). Typical $b_p(\lambda)$ spectra for phytoplankton cultures and phytoplankton-rich natural waters exhibit troughs at wavelengths corresponding to major peaks in the particle absorption spectrum (Bricaud et al. 1988; Babin et al. 2003a; Snyder et al. 2008). In the case of nonalgal particles found in coastal waters, the $b_p(\lambda)$ spectrum often depicts a decreasing trend at short wavelengths of the blue range (e.g., Fig. 1 and Babin et al. 2003a).

Methods

Field measurements—Field measurements were carried out using an absorption and attenuation meter (ac-9, WetLabs) designed with three visible (440, 555, and 630 nm) and six near-IR (715, 730, 750, 767, 820, and 870 nm) spectral channels, and a short path length (10 cm) appropriate for turbid coastal waters.

Measurements were carried out in different European estuarine and coastal waters (Table 1 and Fig. 2). The data set generated by Doxaran et al. (2007), from measurements carried out in the Tamar (southwest England), Elbe (north Germany), and Gironde (France) estuaries, is used in this study. Additional measurements were carried out in the Bristol Channel in August 2006 (23 stations), southern North Sea in September 2006 (19 stations) then July 2007

(19 stations), and northern Baltic Sea in August 2007 (47 stations). The ac-9 sensor was preferably used on the bench just after collecting about 10 liters of water within the surface layer (0–1-m depth). The water sample that passed through the absorption and attenuation tubes was used for further analyses (see paragraphs hereafter).

The ac-9 data were recorded during at least 1 min and averaged to obtain the mean attenuation and absorption spectra for each station. Temperature and salinity were measured simultaneously using a hand thermometer (Hanna Instruments, accuracy: 0.3°C) and a SeaBird SBE-25 sensor, respectively. The ac-9 sensor was rinsed after each measurement and calibrated with Milli-Q water every day to obtain a reference signal and verify the instrument stability.

Temperature and salinity corrections were applied according to standard protocols (Pegau et al. 1997; Sullivan et al. 2006), using temperature correction factors provided by Langford et al. (2001) for the near IR. The “proportional” method was used to correct for residual scattering effects on absorption measurements (Zaneveld et al. 1994). The wavelength 870 nm was used as the reference wavelength where particulate absorption was assumed to be negligible. This assumption is supported by recent measurements obtained with accurate absorption instrumentation having very small scattering error (Babin and Stramski 2004; Stramski et al. 2004, 2007). In the near-IR region (750–850 nm), these studies conclude that absorption by mineral-rich particles is either undetectable or in any case less than 10% of the 400-nm signal. Because of the correction applied to our measurements, light absorption by particles could be recorded between 715 and 870 nm. However, on the basis on Monte Carlo simulations (E. Leymarie unpubl.), the absorption signal recorded by the ac-9 sensor in this near-IR spectral region could result from imperfect correction for residual scattering effects. The particulate scattering coefficient (b_p , in m^{-1}) was finally calculated as:

$$b_p(\lambda) = (c_t[\lambda] - c_w[\lambda]) - (a_t[\lambda] - a_w[\lambda]) \quad (6)$$

where a and c (in m^{-1}) are respectively the absorption and attenuation coefficients and subscripts t and w stand for total and pure water (the ac-9 output values are related to a specific reference medium that is pure water). Errors associated to beam attenuation or b_p measurements when using an ac-9 sensor (10-cm path length) in highly scattering marine environments have been estimated by Piskozub et al. (2004). On the basis of Monte Carlo simulations, these authors showed that errors on b_p only increase from about 18% to 25% when b_p increases from 0.1 to 100 m^{-1} . This is explained by imperfect corrections for forward scattering, whereas errors due to multiple scattering remain limited. On the basis of similar Monte Carlo simulations, E. Leymarie (unpubl.) confirmed these results in the near-IR part of the spectrum and demonstrated that an error associated with the b_p spectral slope measured using an ac-9 device is lower than 5%.

To measure the absorption coefficient of colored dissolved organic matter (a_{CDOM} , in m^{-1}), 1 liter of the

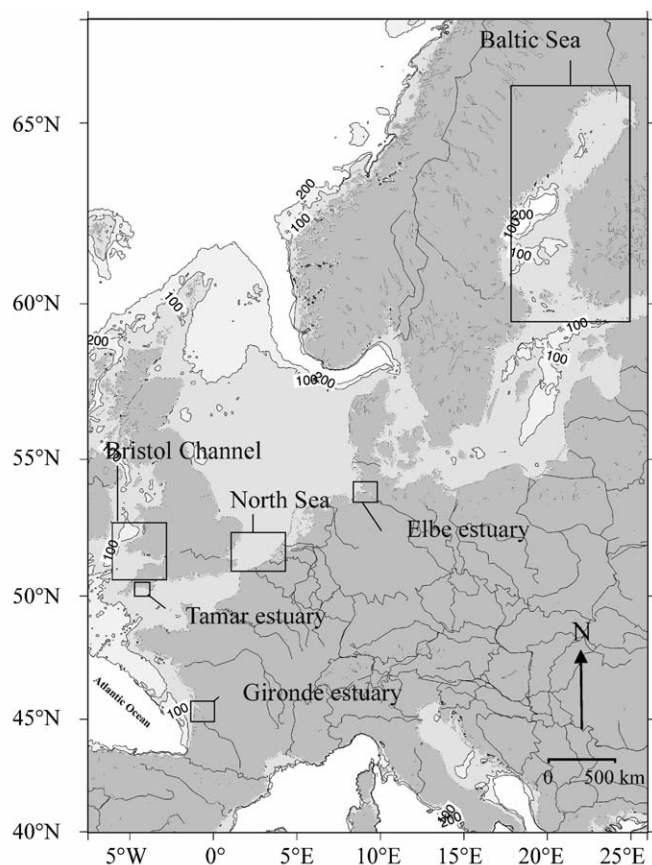


Fig. 2. Location of sampling stations in European coastal and estuarine waters.

water sample exiting the ac-9 was filtered through Whatman Anodisc filters (pore size $0.2 \mu\text{m}$). The a_{CDOM} coefficient was measured between 350 and 750 nm using a spectrophotometer (PerkinElmer Lambda 2) equipped with a 10-cm cuvette, or using the reflective (absorption) tube of the ac-9 sensor. In this latter case, the tube was rinsed twice with Milli-Q water, then once with the filtrate, and filled with the filtrate. The absorption signal of the filtrate was measured, providing $a_{\text{CDOM}}(\lambda)$ after applying corrections for temperature and salinity. The absorption coefficient of suspended particles (a_{p} , in m^{-1}) was finally calculated as the difference:

$$a_{\text{p}}(\lambda) = a(\lambda) - a_{\text{CDOM}}(\lambda) \quad (7)$$

where a is the difference between the total absorption and pure water absorption coefficients.

To determine the concentration of suspended particulate matter (SPM, in g m^{-3}), a known volume of the surface water sample was filtered through preweighed Whatman GF/F filters. Filters stored at -80°C were then dried 24 h at 65°C to obtain the dry weight (Van Der Linde 1998). Filters were finally burned 4 h at 450°C to obtain the dry weight of nonorganic particles.

Several PSD measurements were carried out in the Tamar estuary in 2005, not coincidentally with the ac-9 data. These measurements were made on surface water samples analyzed in the laboratory less than 6 h after collection, using a Coulter counter or a Malvern Mastersizer X. A high determination coefficient ($R^2 > 0.98$) was systematically obtained when Eq. 2 was fitted to the measured PSD (Fig. 3). The exponent of the fitted Junge distribution typically varied between 3.2 and 4.5.

Mie calculations—The particulate scattering and absorption efficiency factors (Q_{b} and Q_{a}) were computed using the code developed by Bohren and Huffman (1983). The PSDs were assumed to follow a Junge distribution (Eq. 2) with a slope (j) ranging from 3.4 to 5 to reproduce PSDs with proportions of coarse and fine particles likely to be present in the marine environment. The assumption of a Junge distribution was also supported by the measurements carried out in the Tamar estuary (Fig. 3). Particle diameters were varied within the size interval $D_{\text{min}} - D_{\text{max}}$ with a ΔD increasing logarithmically from D_{min} to D_{max} . The real part of the refractive index, n , was varied between 1.18 (typical of mineral particles) and 1.05 (typical of biogenic particles or aggregates of fine mineral particles with organic matter and high water content). To a first approximation, the imaginary part of the refractive index, n' , is proportional to the product $\lambda \times a_{\text{p}}(\lambda)$ (Morel and Bricaud 1981; Stramski et al. 2007). We forced the spectral variations of n' to match the measured $a_{\text{p}}(\lambda)$, which typically decreased exponentially from short visible to long near-IR wavelengths, with an exponential slope on the order of 0.013 nm^{-1} . The variations of n' from 440 to 870 nm were accordingly modeled as:

$$n'(\lambda) = n'(440) \times \lambda \times \exp(-0.012 \times [\lambda - 440]) \quad (8)$$

and $n'(440)$ was varied from 0 (nonabsorbing particles) to 0.009 (highly absorbing particles). The 0–0.009 range of $n'(440)$ values is representative for most planktonic and terrigenous mineral-rich particulate matter, but $n'(440)$ values as high as 0.02 have also been documented (Stramski et al. 2001, 2007).

Table 1. Details on field measurements.

Site	Dates	No. of stations	Research vessel and collaborators
Tamar estuary	20–24 Oct 05	16	RV <i>Catfish</i> (University of Plymouth, United Kingdom)
Elbe estuary	31 Oct–02 Nov 05	11	Ferry boat (GKSS, Germany)
Gironde estuary	07–10 Nov 05 and 25–28 Mar 06	38	RV <i>Côte d'Aquitaine</i> (University Bordeaux 1, France)
North Sea	18–22 Sep 06 and 02–06 Jul 07	19	RV <i>Belgica</i> (MUMM, Belgium)
Bristol Channel	07–13 Aug 06	23	RV <i>Prince Madog</i> (University of Strathclyde, United Kingdom)
Baltic Sea	13–24 Aug 07	47	RV <i>Aranda</i> (Finnish Institute of Marine Research, Finland)

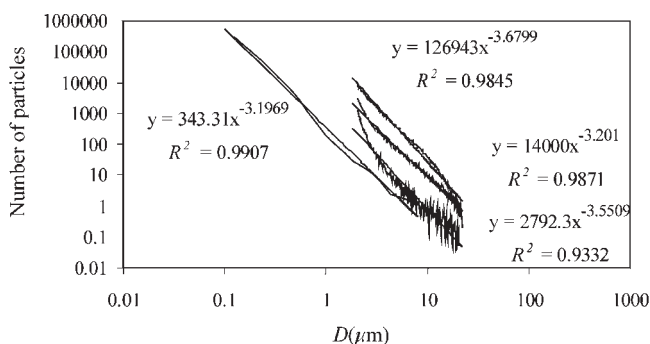


Fig. 3. Typical particle size distributions measured in 2005 on water samples collected within the surface waters of the Tamar estuary, southwest England (i.e., number of particles per size range counted or detected in $0.5 \times 10^{-6} \text{ m}^3$ of water sample). Measurements were carried out in laboratory using a Coulter counter ($2 < D < 20 \text{ } \mu\text{m}$) and using a Malvern Mastersizer X ($0.1 < D < 80 \text{ } \mu\text{m}$). A power-law function (Eq. 2) was fitted to each measurement.

The total volume of particles per volume of water was fixed to the same value in all computations. This removed the influence of changing suspended particle volume (or mass) concentration in water. Computations were made for the visible and near-IR wavelengths of our ac-9 sensor (440, 555, 630, 715, 730, 750, 767, 820, and 870 nm) to facilitate direct comparison with measurements. Inputs for Mie computations are summarized in Table 2.

The final step was to select the appropriate size range $D_{\min} - D_{\max}$ to capture almost entirely the quantity $b_p(\lambda)$ in Eq. 3 when taking into account the variations of λ , m , and j . To capture the contributions of both small and coarse particles independently of the j exponent, D_{\min} and D_{\max} were set to constant values of $0.02 \text{ } \mu\text{m}$ and $600 \text{ } \mu\text{m}$, respectively. This size range, slightly wider than the range of $0.05\text{--}500 \text{ } \mu\text{m}$ considered by Woźniak and Stramski (2004), who modeled the optical properties of mineral particles suspended in seawater, remained unchanged through all calculations.

Results

Analysis of the data set—Surface *SPM* concentrations measured in the various study areas cover a wide range, $1\text{--}345 \text{ g m}^{-3}$ (Table 3). The highest concentrations were found in the Gironde and Elbe estuaries, due to the presence of maximum turbidity zones. Generally lower concentrations were measured in the Tamar estuary, North Sea, and Bristol Channel, where the data set includes stations in more open coastal waters. The minimum *SPM* concentrations were found in the Baltic Sea. Low and stable particulate organic contents were observed in the Gironde and Elbe estuaries (around 10% of the total mass of suspended matter), due to direct river inputs of mineral particles trapped in the maximum turbidity zones (Table 3). Higher particulate organic contents and variations were found in the Bristol Channel. The suspended particles in the Tamar estuary showed a rather high organic content

Table 2. Inputs for Mie calculations.

n_w (independent of λ)	1.34 (seawater refractive index)
n (independent of λ)	1.05 and 1.18
n' at 440 nm (Eq. 8)	0, 0.001, 0.002, 0.004, 0.006, 0.009
D_{\min} and D_{\max} (μm) (Eq. 3 and 3')	0.02 and 600
j (Eq. 2)	3.4, 3.6, 3.8, 4.0, 4.5, 5.0
λ (nm)	440, 555, 630, 715, 730, 750, 767, 820, 870

(28% of the total mass of suspended matter, on average, and up to 58% in the mouth area). In the Baltic Sea, suspended particles were mainly organic (from 60% to 100% of the total *SPM* mass). A wide range of suspended particles was therefore sampled and analyzed, so the resulting data set can be assumed to be representative of various coastal waters and types of particles of coastal origin.

For a first impression of the optical properties of the particles sampled in the different study areas, we examined the variations of the particulate single-scattering albedo $\omega_p(\lambda)$ defined as the ratio $b_p(\lambda):c_p(\lambda)$ where b_p and c_p (in m^{-1}) are respectively the particulate scattering and attenuation coefficients. Results are presented at 440 nm where particulate absorption and scattering properties are both significant (Fig. 4). The particles sampled in the Elbe and Gironde waters, but also in the coastal waters of the North Sea, were highly scattering, with $\omega_p(440)$ values higher than 0.8 and even close to 1. The particles found in the Tamar, Bristol Channel, and Baltic Sea waters, but also in the North Sea away from the coasts, proved to be less specific, with $\omega_p(440)$ values varying in the range 0.7–1, i.e., predominantly scattering particles with significant absorption properties. The full data set covers a rather wide range of particulate absorption and scattering properties that are typical of turbid coastal waters. A similar though wider range of $\omega_p(440)$ values (0.6–1) is obtained with our Mie computations.

To highlight the variability in spectral variations of the $b_p(\lambda)$ spectrum observed in the different sampled areas, the measured b_p spectra are normalized at 870 nm (Fig. 5). In the near IR, independently of the study area, rather smooth spectral variations are systematically observed. The steepest spectral variations are observed in the Tamar estuary and Baltic Sea (b_p values smoothly increasing from near IR to short visible wavelengths). A wider range of spectral variations is found in the Gironde and Elbe estuaries: steep variations as in the Tamar, but also rather flat spectra with sometimes decreasing b_p values at short visible wavelengths. This decrease of b_p at short visible wavelengths is highly pronounced on the North Sea and Bristol Channel data where a discontinuity is systematically observed at 440 nm. This wavelength corresponds to strong light absorption by both phytoplankton and nonalgal particles. This decrease of b_p values at visible wavelengths corresponding to high particulate absorption was previously observed in field and laboratory data (Babin et al. 2003a; Stramski et al. 2007). A similar decrease was also documented by Snyder et al. (2008) (see their fig. 2), who

Table 3. Site-by-site minimum, maximum, average, and standard deviation (SD) of the measured *SPM* concentration (in g m^{-3}) and mass ratio of organic to dry particulate matter ($SPM_{\text{org}}:SPM$, in percentage).

Region	<i>n</i>	<i>SPM</i> (g m^{-3})				$SPM_{\text{org}}:SPM$ (%)			
		Min.	Max.	Average	SD	Min.	Max.	Average	SD
Tamar	16	4.0	47.1	17.6	12.6	8.8	57.6	27.9	11.6
Elbe	11	73.5	294.2	166.4	67.5	9.2	12.0	10.3	1.2
Gironde	38	21.9	344.1	141.4	83.0	5.8	13.4	9.5	2.3
North Sea	19	0.8	36.5	11.5	11.4	-	-	-	-
Bristol Channel	23	2.8	77.2	13.0	18.5	5.2	28.9	15.2	6.7
Baltic Sea	47	0.9	4.3	2.1	0.8	59.0	99.6	93.3	10.4

even obtained a negative γ slope when fitting Eq. 4 to their b_p measurements. In our b_p values extended to the near IR, artifacts are sometimes observed between 730 and 750 nm, where light absorption by pure water is highly sensitive to water temperature (Langford et al. 2001; Sullivan et al. 2006) (see the spectra measured in the North Sea and Bristol Channel on Fig. 5).

The mass-specific particulate scattering coefficient ($b_p^*[\lambda]$ in $\text{m}^2 \text{g}^{-1}$) is defined as the particulate scattering coefficient per unit of *SPM* concentration. At 555 nm, $b_p^*(555)$ exhibits significant region-to-region variations ($0.35\text{--}0.57 \text{ m}^2 \text{g}^{-1}$) around a mean value of $0.43 \text{ m}^2 \text{g}^{-1}$ (Table 4). The highest $b_p^*(555)$ values are observed in the Tamar, with strong local variations. These b_p^* variations may be related to the variations of the particulate organic content observed in this area (Table 3). Rather similar mean $b_p^*(555)$ values (around $0.40 \text{ m}^2 \text{g}^{-1}$) are observed in the other study areas. These values are rather stable in the Elbe, Gironde, Baltic Sea, and North Sea. In contrast, important variations are found in the Bristol Channel, where significant variations of the particulate organic content are observed (Table 3). Overall and site by site, similar variations and slightly lower values of b_p^* are obtained at 715 nm. The mean $b_p^*(715)$ values are typically $0.32 \pm 0.04 \text{ m}^2 \text{g}^{-1}$, excluding the Tamar data set. Globally our values are concordant with those reported by Babin et al. (2003a) for various European coastal waters (mean $b_p^*[555]$ values of 0.51 and $0.56 \text{ m}^2 \text{g}^{-1}$ for their entire and channel data sets, respectively).

A similar analysis is made concerning the mass-specific particulate absorption coefficient ($a_p^*[\lambda]$ in $\text{m}^2 \text{g}^{-1}$), i.e., the particulate absorption coefficient per unit of *SPM* concentration. Strong region-to-region and regional variations are observed (Table 5). Typical variations at 440 nm, e.g., from 0.041 (North Sea) to $0.058 \text{ m}^2 \text{g}^{-1}$ (Elbe), are in the range documented by Babin et al. (2003b) or McKee and Cunningham (2006) for nonalgal particles in European coastal waters ($0.033\text{--}0.067 \text{ m}^2 \text{g}^{-1}$ at 443 nm). Higher $a_p^*(440)$ values are observed in the Tamar and Baltic Sea (mean value of $0.088 \text{ m}^2 \text{g}^{-1}$), where particles were predominantly organic. Such values are higher than those previously documented by Babin et al. (2003b) in the southern Baltic Sea, but still lower than those measured by Dall'Olmo and Gitelson (2005) in highly productive lake waters.

Spectral slope of the particulate scattering coefficient in the near IR—We first analyze the spectral slope of the

particulate scattering coefficient in the near-IR (715–870 nm) region. The spectral dependence of $b_p(\lambda)$ is fitted to the power law (Eq. 4):

$$b_p(\lambda) = b_p(715)(\lambda/715)^{-\gamma} \quad (9)$$

The scattering spectral slope γ is retrieved by minimizing the sum of the squared differences between the modeled (Eq. 9) and measured $b_p(\lambda)$ values. Only the near-IR 715-, 730-, 750-, 767-, 820-, and 870-nm wavelengths are considered, and γ is allowed to vary in a wide range, $-1\text{--}2$.

The results show the validity of Eq. 9, which fits the measured b_p spectra with a determination coefficient (R^2) higher than 0.95 in all the study areas. For comparison, Doxaran et al. (2007) obtained a mean R^2 coefficient of 0.99 when only estuaries were considered. A wide range of γ spectral slope is observed in the North Sea, Bristol Channel, and Baltic Sea ($0.35\text{--}1.10$, $0.10\text{--}1.20$, and $0.40\text{--}1.30$, respectively). On the basis of Eqs. 2, 4, and 5, this could result from either change in the slope of the PSD represented by a Junge distribution or alternatively a significant deviation from a Junge size distribution.

The variations of γ are analyzed as a function of water turbidity (here $b_p[715]$ is used as a proxy) (Fig. 6). Results show a trend between γ and the level of light scattering or, equivalently, the concentration of suspended particles. The γ values encountered in highly turbid estuarine waters ($b_p[715] > 10 \text{ m}^{-1}$) vary around a mean value of 0.4 ± 0.3 (Gironde, Elbe). In moderately turbid waters ($1 < b_p[715] < 10 \text{ m}^{-1}$), wide variations in γ are observed (0.6 ± 0.5), which suggests differences in PSDs between the Bristol Channel, North Sea, and Tamar, respectively. These results are consistent with previous observations (Doxaran et al. 2007). In the clearest waters sampled ($b_p[715] < 1 \text{ m}^{-1}$), the γ slope clearly increases with decreasing turbidity but also with increasing water depth for the Bristol Channel, North Sea, and Baltic Sea (not shown). This might be related to the settling of coarse mineral particles close to their sources (river mouths and mud banks along the coast), or it could be that mineral particles did not completely dominate the scattering signal in surface waters for deeper stations. On the basis of available observations, water turbidity appears as the predominant factor with which γ covaries.

How different are the particulate scattering spectral slopes in the visible and near IR?—Mie computations are first used

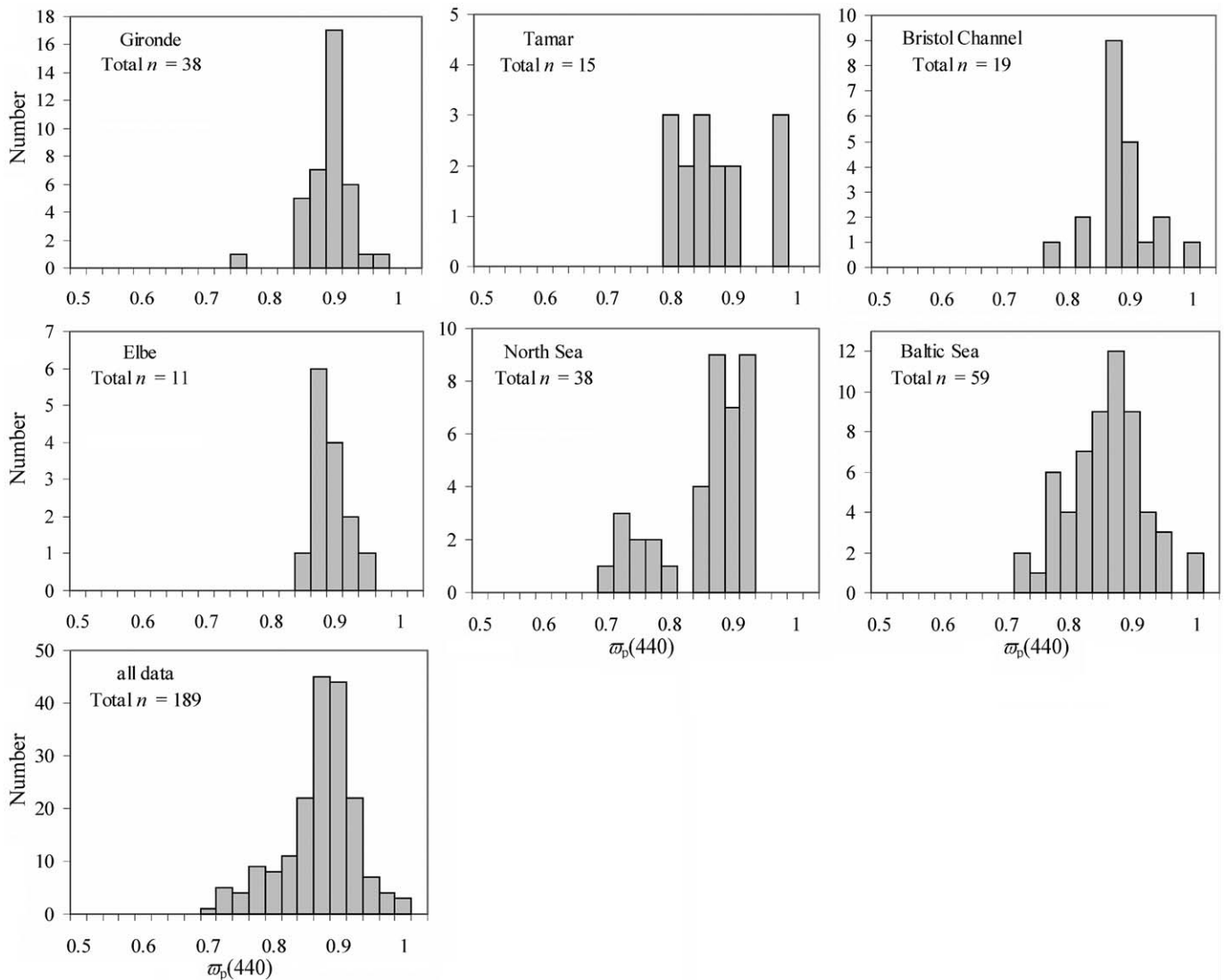


Fig. 4. Site-by-site and overall histogram plots of the particulate single-scattering albedo $\omega_p(440) = (b_p : [a_p + b_p])(440)$, a_p and b_p (in m^{-1}) being respectively the particulate absorption and scattering coefficients.

to assess the differences between the near-IR and visible b_p spectral slopes in the case of nonabsorbing particles, then in the case of particles increasingly absorbing light toward short visible wavelengths (using Eq. 8 to generate n'). Visible wavelengths where light absorption by particles is low are first considered (i.e., the wavelength 440 nm is avoided). The γ spectral slope (Eq. 9) is calculated within the visible (555, 630, and 715 nm) and near-IR (715, 730, 750, 767, 820, and 870 nm) spectral domains. Several important remarks can be made on the basis of results obtained (Fig. 7).

First and as expected, the γ spectral slope is the same in the visible and near IR when the particles are nonabsorbing (Fig. 7). In this case, the γ spectral slope is only related to the PSD according to Eq. 5. The range $D_{\min} - D_{\max}$ was therefore appropriately selected so that the integral (Eq. 3) captured almost entirely the quantity $b_p(\lambda)$. Actually, the γ spectral slope calculated for a j value

of 3.4 is slightly higher than 0.4 when n is 1.18 (4.1) and even higher when n is 1.05 (4.15). For such a size distribution, the contribution to light scattering of particles with a diameter of $600 \mu m$ is still significant and D_{\max} should be set above this value. The Mie code used in this study does not allow it, as the particle diameter becomes too high compared with the wavelength of light. However, this very slight underestimation of light scattering by coarse particles has a negligible effect on our analyses and interpretation.

As particles increasingly absorb light, the γ slope decreases significantly in the visible and rather slightly in the near IR, so that the scattering slopes in the visible and near IR differ (Fig. 7). This simply results from the spectral variations selected for n' , i.e., increasing values toward short visible wavelengths (Eq. 8), as previously observed on the basis of Mie calculations (*see* fig. 4e,f in Woźniak and Stramski 2004). Another important point is that particulate

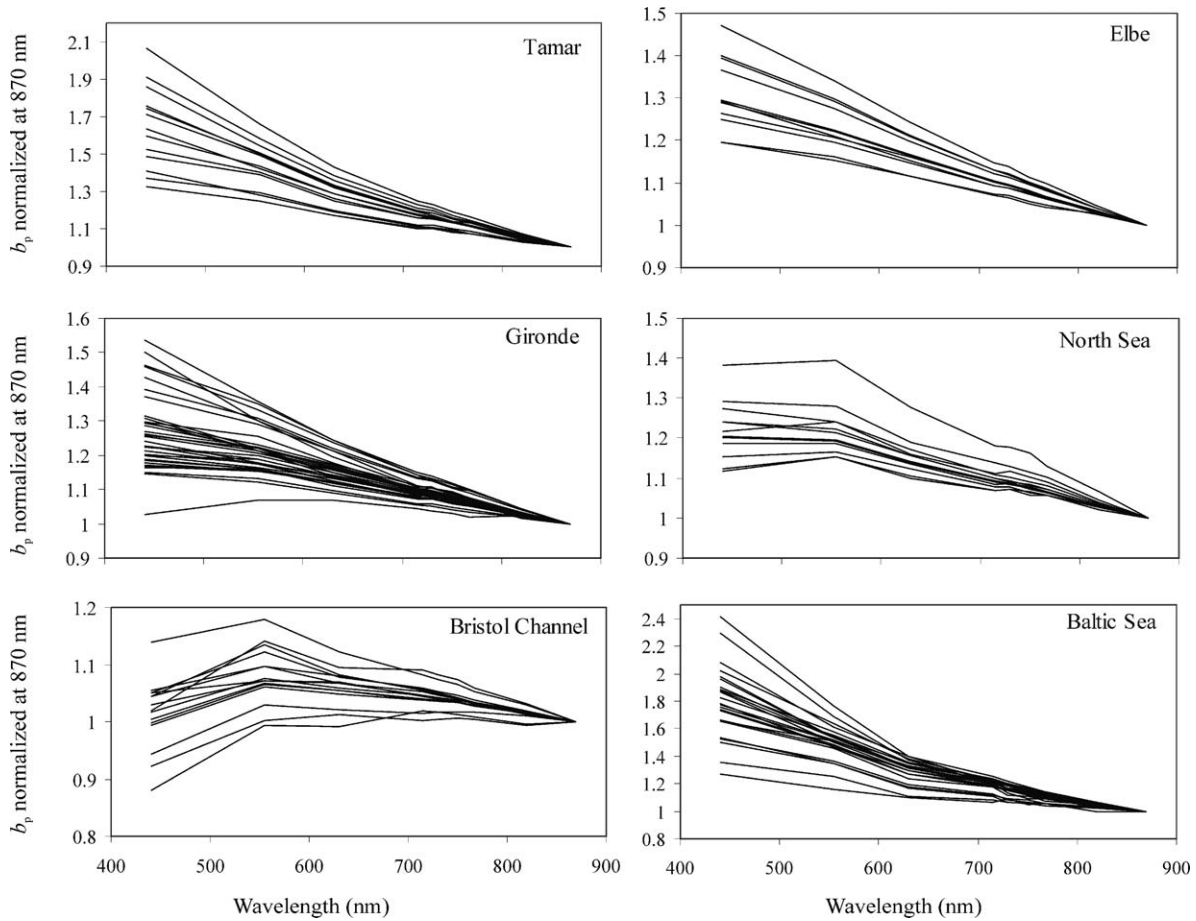


Fig. 5. Typical site-by-site measured b_p spectra (normalized at 870 nm).

absorption effects on scattering decrease when j increases, i.e., when the proportion of fine particles grows. The explanation is related to the interplay of variations in both Q_a and Q_b with particle size (here the particle diameter, D) (Morel and Bricaud 1981). At a fixed wavelength and for a given value of the particle refractive index, as D increases, Q_a increases gradually from almost 0 to 1 while Q_b first increases and remains higher than Q_a , reaches a maximum value, then oscillates and converges toward the value of 1 (equal to Q_a). When the value of the slope j is higher than

4.0 and even close to 5.0 (high proportion of fine particles), the size range of submicrometric particles little influenced by absorption effects (low Q_a) mainly contributes to the scattering coefficient b_p . By opposition, when the proportion of coarse particles increases (decreasing j values), mid-size particles ($D > 1 \mu\text{m}$) directly influenced by absorption effects (Q_a increasing toward 1) mainly contribute to the particle-scattering coefficient. This explains why particulate absorption effects on particulate scattering decrease with decreasing particle size.

Table 4. Global and site-by-site statistics of the mass-specific particulate scattering coefficient, i.e., the $b_p(\lambda):SPM$ ratio ($\text{m}^2 \text{g}^{-1}$). Averages and standard deviations (SD) are presented at two wavelengths.

Region	n	Wavelength			
		555 nm		715 nm	
		Average	SD	Average	SD
		$(\text{m}^2 \text{g}^{-1})$		$(\text{m}^2 \text{g}^{-1})$	
Tamar	16	0.57	0.11	0.47	0.10
Elbe	11	0.41	0.06	0.38	0.06
Gironde	38	0.39	0.11	0.36	0.09
North Sea	19	0.35	0.08	0.31	0.08
Bristol Channel	23	0.38	0.17	0.35	0.13
Baltic Sea	47	0.41	0.09	0.33	0.08
All	154	0.43	0.17	0.37	0.15

Table 5. Global and site-by-site statistics of the mass-specific particulate absorption coefficient, i.e., the $a_p(\lambda):SPM$ ratio ($m^2 g^{-1}$). Averages and standard deviations (SD) are presented at three wavelengths.

Region	n	Wavelength					
		440 nm		555 nm		715 nm	
		Average	SD	Average	SD	Average	SD
		$(m^2 g^{-1})$		$(m^2 g^{-1})$		$(m^2 g^{-1})$	
Tamar	16	0.088	0.045	0.029	0.016	0.019	0.006
Elbe	11	0.058	0.014	0.024	0.004	0.013	0.005
Gironde	38	0.042	0.017	0.018	0.008	0.008	0.004
North Sea	19	0.041	0.026	0.013	0.016	0.007	0.008
Bristol Channel	23	0.055	0.038	0.023	0.013	0.011	0.007
Baltic Sea	47	0.088	0.035	0.051	0.031	0.009	0.008
All	154	0.071	0.038	0.026	0.016	0.011	0.007

Finally, particulate absorption effects on scattering significantly increase with decreasing values of n . This is related to the variations of both Q_a and Q_b with respect to the particle diameter. As n varies from 1.18 to 1.05, the maximum efficiency for light scattering shifts significantly toward coarse particles, which are more affected by particulate absorption (high Q_a values). Light scattering by mineral particles ($n = 1.18$) is therefore less influenced by particulate absorption than particles with a low refractive index (e.g., $n = 1.05$).

As light absorption by marine particles is low and almost negligible in the near IR, it can be concluded that Eq. 4 is robust in this spectral domain. Eq. 4 may also be approximately valid in the visible region for fine particles even if they significantly absorb light. However, departure from Eq. 4 systematically occurs in the visible in the case of coarse absorbing particles. This departure is even more significant if particles have a real refractive index close to 1.

Field data are finally used to compare the γ spectral slopes of b_p in the visible (555, 630, and 715 nm) and near-IR (715, 730, 750, 767, 820, and 870 nm) spectral domains (as in Fig. 7 for Mie computations). Equation 9 was fitted

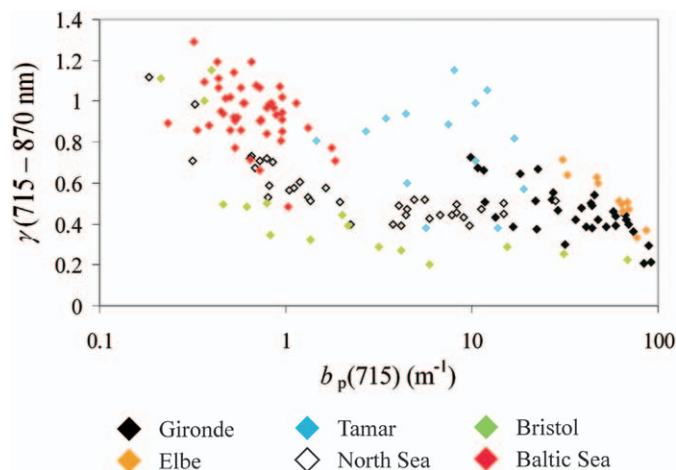


Fig. 6. Plot of the measured b_p spectral slopes in the (715–870 nm) near-IR spectral region (Eq. 9) as a function of $b_p(715)$, used as a proxy for water turbidity.

using the b_p values measured at 555, 630, and 715 nm and the determination coefficient was systematically higher than 0.90. Equation 9 was thus also appropriate in this visible spectral range for the selected wavelengths. The results obtained indicate that the γ spectral slope is typically lower in the visible than in the near IR (Fig. 8). The points are scattered under the 1:1 relationship, with some regional differences, but globally the relationship obtained is linear, with a slope close to 1 and a significant intercept of -0.0923 . The observed relative differences between the near-IR and visible b_p spectral slopes remain limited in the case of high near-IR γ values (i.e., predominantly fine particles) but greatly increase in the case of low near-IR γ values (i.e., predominantly coarse particles). This was

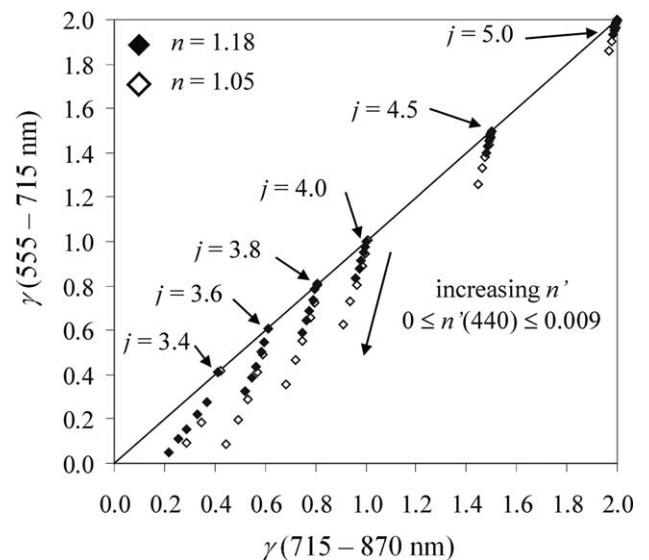


Fig. 7. Plot of the visible (555–715 nm) b_p slope as a function of the near-IR (715–870 nm) b_p slope, on the basis of Mie computations. The corresponding Junge exponents (j) of the particle size distribution are indicated on the graph. Results are presented for two real parts of the particle refractive index, n : 1.18 and 1.05. The points corresponding to nonabsorbing particles ($n' = 0$) are on the 1:1 relationship, then points increasingly depart from this relationship, with $n'(440)$ values increasing in the range 0.001–0.009.

expected from Mie computations (Fig. 7). The overall relationship obtained from field data may be used to estimate the near-IR γ slope from historical b_p measurements made for visible wavelengths.

On the basis of these first results, we conclude that particulate absorption effects on the scattering are always significant in the visible, even when wavelengths associated with high particulate absorption are avoided. A unique power-law function (e.g., Eq. 9) cannot be used to model the b_p spectral variations from the near IR toward the visible (Eck et al. 1999). Further investigations are needed concerning these particulate absorption effects to propose an improved model of the $b_p(\lambda)$ spectrum in the visible.

New approach for modeling the particulate light-scattering coefficient in the visible region—In this section, the particulate scattering coefficient of nonabsorbing particles is denoted b_{pna} . The b_{pna} values are obtained by assuming that measured near-IR b_p values effectively represent b_{pna} at these wavelengths and Eq. 9 can be used to extrapolate to visible wavelengths. The particulate scattering coefficient of absorbing particles is denoted by b_p , and the difference from Eq. 9 due to absorption effects is written (see Fig. 1):

$$\Delta b_p(\lambda) = b_{\text{pna}}(\lambda) - b_p(\lambda) = f(a_p) \quad (10)$$

On the basis of field data, we first examine the difference between b_p and b_{pna} at the shortest visible wavelength available (440 nm). At this wavelength, particulate absorption was observed to be at a maximum (see Table 5), so that the particulate absorption effects on b_p were also expected to be at a maximum. The ratio $\Delta b_p : b_{\text{pna}}$ at 440, expressed in percentage, was therefore used to quantify the departure of b_p from b_{pna} , i.e., to quantify the errors that can be committed when using a power-law function to model the spectral variations of b_p in the visible. The results clearly show a significant departure, in a range varying from 1% to 35%, that slightly increases with decreasing values of the b_p near-IR spectral slope (Fig. 9). The mean departure varies from one region to another and is higher than 10% for the overall data set.

Our previous results (e.g., Fig. 7) suggest that the difference Δb_p covaries with the particulate absorption coefficient (a_p) but also depends on the particle size distribution and composition (i.e., the real part of the refractive index, n). The Mie computations are used to express Δb_p as a function of a_p for different PSD and real refractive indices of the particles. The same size intervals (D_{min} , D_{max}) are used to compute b_p (Eq. 3) and a_p (Eq. 3'). All the visible but also near-IR wavelengths are considered. Results (Fig. 10) are presented separately for each PSD (Junge-type PSD with a slope j of 3.4, 3.6, 3.8, 4.0, and 5.0, and n values of 1.05 and 1.18). Note that a_p typically increases with increasing j value, i.e., with the proportion of fine particles. This is due to the packaging effect (Morel and Bricaud 1981). Note also that Δb_p increases when j varies from 3.4 to 4.0, then decreases when j varies from 4.0 to 5.0, which is due to the variations of b_p with j (for a constant volume or mass of particles following a Junge size distribution, the magnitude of b_p is maximum when j is

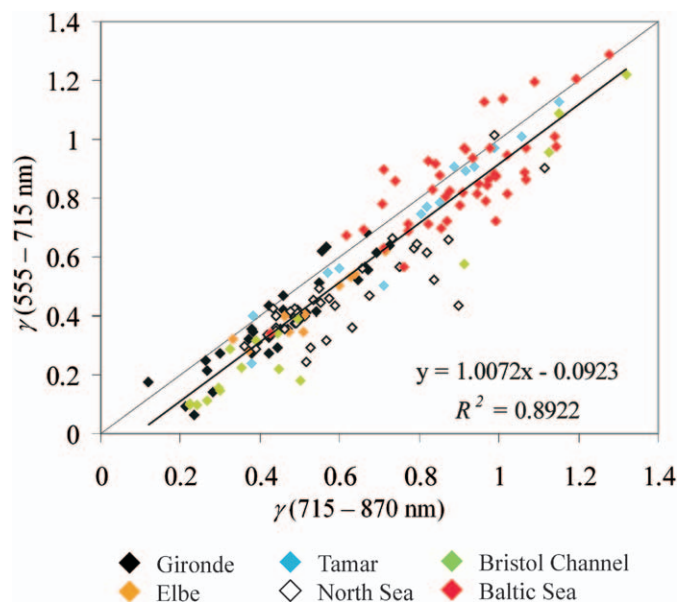


Fig. 8. Plot of the visible (555–715 nm) b_p slope as a function of the near-IR (715–870 nm) b_p slope, on the basis of field measurements. The gray and black straight lines show respectively the 1:1 relationship and best-fitted linear relationship with the corresponding equation and determination coefficient (R^2).

equal to 4.0). A linear relationship with a null intercept is systematically obtained between Δb_p and a_p for a given set of j and n values. For a high proportion of coarse particles ($j = 3.4$), the difference Δb_p is almost equal to a_p , almost independently of the wavelength and n . As the proportion of fine particles increases ($j \geq 3.6$), Δb_p becomes progressively lower than a_p and the influence of n on the relationship between Δb_p and a_p is more significant. The difference Δb_p finally becomes almost negligible when the proportion of very fine particles is maximum ($j = 5.0$). Light scattering by small particles is therefore little affected by particulate absorption.

To determine whether these results are still valid when phytoplankton particles dominate, we carried out additional Mie calculations. We used as inputs typical values of phytoplankton refractive index (Stramski et al. 2001): $n = 1.05$; $n'(440) = 0.0026$, $n'(675) = 0.002$, and the spectral variations of $n'(\lambda)$ shown by Babin et al. (2003a) (see their fig. 8). We also considered additional wavelengths (412, 490, and 676 nm) to reproduce the complex spectral variations of phytoplankton pigments. Phytoplankton particles were first assumed to follow a Junge-type size distribution. The results obtained (Fig. 10B) confirm that Δb_p still varies as a function of a_p , following a linear relationship with null intercept. As long as the PSD is hyperbolic (Junge law) and independently of the spectral variations of a_p , the slope of this linear relationship mainly depends on the Junge exponent, i.e., the proportions of small and large particles.

A more realistic case of mixed populations of marine detrital and phytoplankton particles was then considered. Detrital particles ($n = 1.05$ and $n'[\lambda] = 0.007954 \exp[-0.007186 \lambda]$, on the basis of Woźniak and Stramski [2004]) were assumed to follow a Junge-type size distribu-

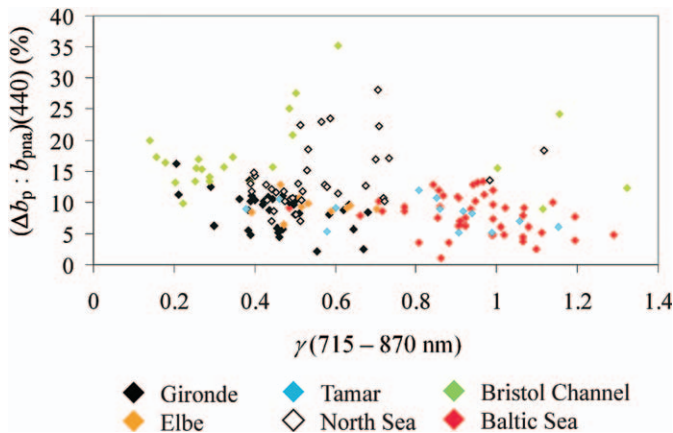


Fig. 9. Plot of the measured $(\Delta b_p : b_{pna})(440)$ ratio, expressed in percentage, as a function of the $b_p(715\text{--}870\text{ nm})$ spectral slope. The $b_{pna}(440)$ value was obtained when applying a power-law function (Eq. 4) using the measured $b_p(870)$ value and $b_p(715\text{--}870\text{ nm})$ spectral slope.

tion (j slopes of 3.4, 3.8, and 5.0) and to represent 90% of the total volume of particles. The size distribution of phytoplankton particles (same refractive index as in Fig. 10B) was modeled using a log-normal function with a mean diameter and standard deviation of $3\ \mu\text{m}$ and $1.2\ \mu\text{m}$, respectively, representing 10% of the total volume of particles. The result was Junge-type PSDs with “a bump” around $3\ \mu\text{m}$ that satisfactorily matched PSDs measured in phytoplankton-dominated waters of the South Pacific Ocean (A. Sciandra pers. comm.). As a first approximation, the obtained relationship between Δb_p and a_p is still linear with null intercept (Fig. 10C). The slope of this relationship decreases as the Junge exponent j (detrital particles) increases from 3.4 to 5.0, but this decrease is moderate due to the presence of phytoplankton particles with a fixed size distribution. The results obtained are therefore apparently robust, i.e., almost independent of the wavelength and particle refractive index, as long as the PSD is close to a Junge-type size distribution.

Another preliminary conclusion is that the effects of particulate absorption can be easily modeled, as $b_p(\lambda) \approx b_{pna}(\lambda) - a_p(\lambda)$, when the proportion of coarse particles is high enough (e.g., a Junge-type PSD with a slope j of 3.4). But overall, these absorption effects are a complex function of a_p , n , and the PSD. On the basis of these results, the modeling of $b_p(\lambda)$ in the visible spectral domain is necessarily complex as it should take into account the particle size distribution and composition. At this stage, the difference Δb_p can simply be written as:

$$\Delta b_p(\lambda) \leq a_p(\lambda) \quad (11)$$

As the ratio $(\Delta b_p : a_p)$ is a constant for a given set of j and n values (Fig. 10), $(\Delta b_p : a_p)$ can be plotted as a function of j (or γ according to Eq. 5) for different n values. Such a plot is presented in Fig. 11A for the two extreme n values considered (1.05 and 1.18). A rather narrow envelope is obtained that depicts the decrease of $(\Delta b_p : a_p)$ with increasing γ values. The width of the envelope is determined

by the particle composition, through the n value. The relationship between $(\Delta b_p : a_p)$ and γ is not linear and can be closely reproduced by using the following equation:

$$\Delta b_p / a_p = 1 - \tanh(0.5 \times \gamma^2) \quad (12)$$

where the 1 and 0.5 constants correspond to a mean value of the real refractive index ($n = 1.10$). These constant values are slightly different for n values of 1.05 or 1.18.

On the basis of the wide range considered for γ (0–2), it clearly appears that the simple assumption $\Delta b_p(\lambda) \approx a_p(\lambda)$ systematically overestimates the particulate absorption effects and would result in significant errors when modeling $b_p(\lambda)$.

To test whether our field data fit these theoretical results, the measured near-IR b_p coefficients are assumed to represent the case of nonabsorbing particles. Equation 9 is fitted to the b_p values measured between 715 and 870 nm and the fitted function is extrapolated to the whole spectral region considered (440–870 nm) to estimate $b_{pna}(\lambda)$ in the visible. The difference Δb_p is then calculated as the difference between the estimated b_{pna} and measured b_p values (see Fig. 1). Only the 440-nm wavelength is considered here to limit the noise due to a_p measurement uncertainties. The measured $(\Delta b_p : a_p)(440)$ ratios are plotted as a function of the measured near-IR γ slopes, over the theoretical envelope obtained from Mie computations (Fig. 11B). On this plot, only measurements where the near-IR γ slope was obtained with a determination coefficient (R^2) higher than 0.98 are considered. This removes the influence of inaccurate b_{pna} values, and thus Δb_p differences, obtained at 440 nm through extrapolation from the near IR. This still represents more than 85% of the data set. The results obtained are conclusive: most of the measurements are included inside the theoretical envelope and follow the predicted decrease of $(\Delta b_p : a_p)$ with increasing γ values. Despite the noise due to residual measurement uncertainties, it can be concluded that the assumptions made concerning the PSDs (e.g., Junge size distributions) were acceptable and that particulate absorption effects on particulate scattering can be modeled using Eq. 12, to a first approximation.

To confirm this result and assess the improvement provided by this new b_p spectral model, the departure of b_p from b_{pna} at 440, expressed as $(\Delta b_p : b_{pna})(440)$, in percentage, is re-examined using our field data set. The departures from a simple power-law function initially observed (Figs. 9, 12A) are first compared with the ones obtained when assuming $\Delta b_p = a_p$. In this latter case, the departures are calculated using the ratio $(\Delta c_p : b_{pna})(440)$, i.e., $(b_{pna} - b_p - a_p) : b_{pna}$ at 440 nm (Fig. 12B). Then the departures are calculated using the ratio $(\Delta b_{p\text{cor}} : b_{pna})(440)$, i.e., $(b_{pna} - b_p - [1 - \tanh(0.5 \times \gamma^2)] \times a_p) : b_{pna}$ at 440 nm (Fig. 12C). Again the results are conclusive. When the particulate absorption effects on $b_p(\lambda)$ are ignored, the actual $b_p(440)$ values are overestimated by 11% on average and by up to 35% (Fig. 12A). When the particulate absorption effects are corrected by assuming $\Delta b_p = a_p$, the actual $b_p(440)$ values are underestimated by 5% on average and by up to 31% (Fig. 12B). This simple

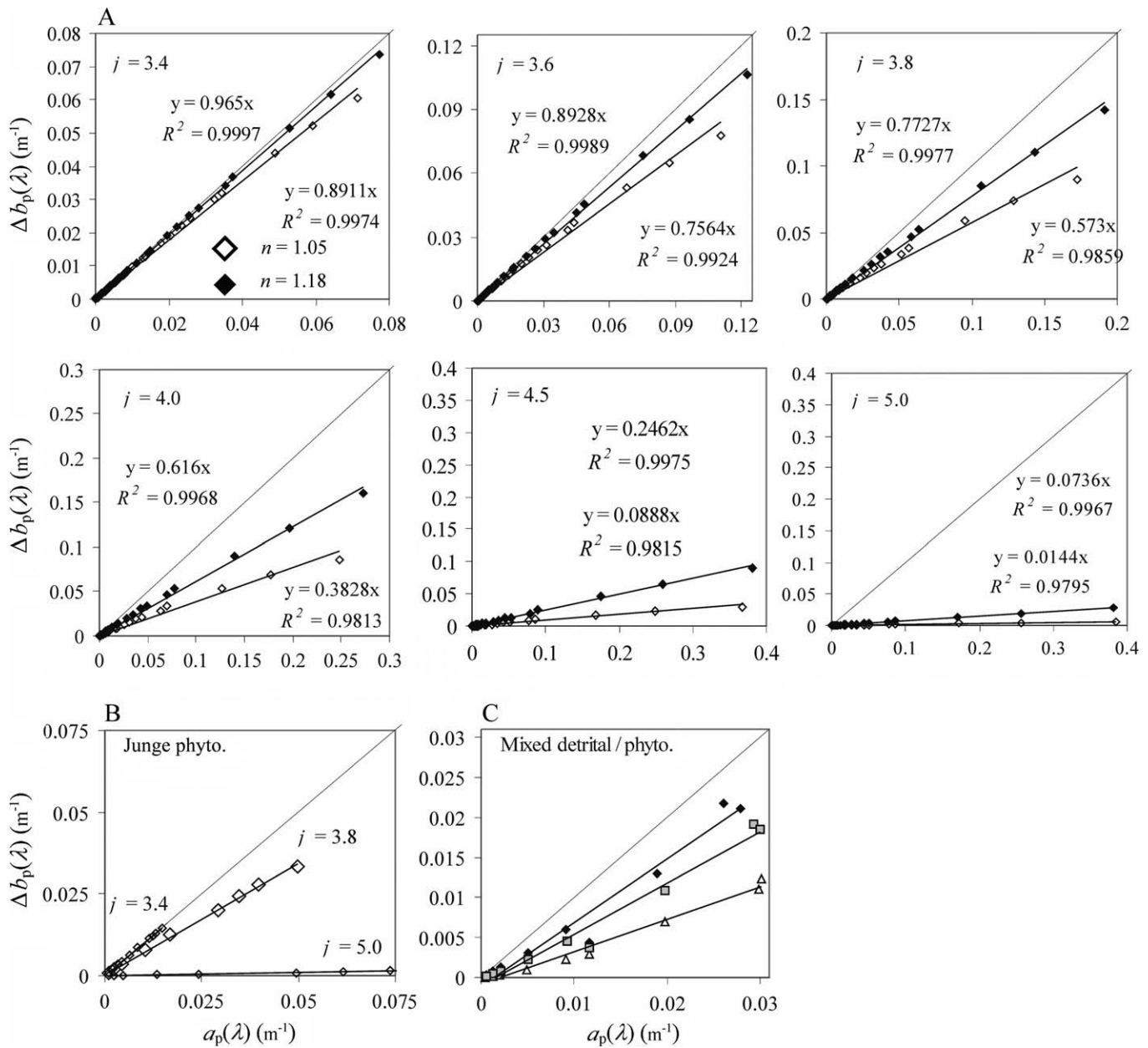


Fig. 10. Plot of $\Delta b_p(\lambda)$ as a function of $a_p(\lambda)$, on the basis of Mie calculations. Results are presented for (A) two values of the real refractive index, n : 1.05 and 1.18; the imaginary refractive index at 440 nm, $n'(440)$, varies from 0.001 to 0.009, and n' varies spectrally according to Eq. 8, with $440 < \lambda < 870$ nm; the PSDs were modeled using a Junge-type function with a slope j increasing from 3.4 to 5.0. (B) A typical refractive index of phytoplankton: $n = 1.05$; $n'(440) = 0.0026$, $n'(675) = 0.002$ and the spectral variations of $n'(\lambda)$ are those shown by Babin et al. (2003a) (see their fig. 8), with $440 < \lambda < 870$ nm. The PSDs were modeled using a Junge-type function with j slope of 3.4, 3.8, and 5.0. (C) Mixed populations of marine detrital particles ($n = 1.05$ and $n'[\lambda] = 0.007954 \exp[-0.007186 \lambda]$) and phytoplankton (refractive index defined as in [B]), with $4412 < \lambda < 870$ nm. The size distributions of marine detrital particles were modeled using a Junge-type function with j slopes of 3.4 (black diamonds), 3.8 (gray squares), and 5.0 (white triangles). The size distribution of phytoplankton was modeled using a log-normal function (mean diameter of 3 μm and standard deviation of 1.2 μm). The detrital and phytoplankton particles represented 90% and 10% of the total volume of particles, respectively.

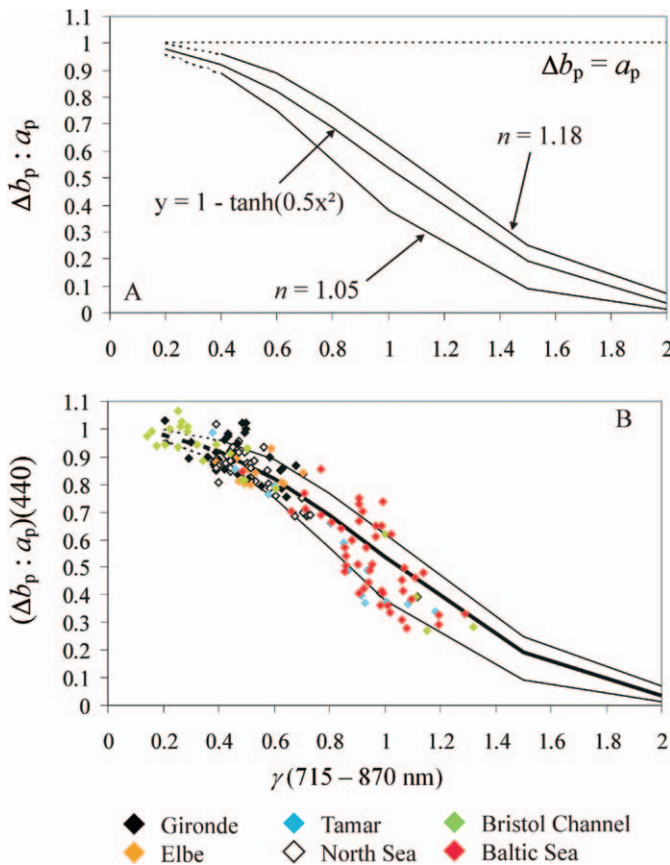


Fig. 11. (A) Theoretical variations of $\Delta b_p : a_p$ as a function of the b_p (715–870 nm) spectral slope (γ). Results were obtained using Mie calculations assuming Junge-type PSDs defined by their exponent j and for two values of the real refractive index, n : 1.05 and 1.18 (see the text for detailed model inputs). The thick straight line shows the mean regression. (B) Overplot of the $(\Delta b_p : a_p)(440)$ values measured in the different study areas.

correction is satisfactory only when the near-IR slope γ is lower than 0.5. Finally, when the correction proposed in Eq. 12 is applied, the relative errors associated with the retrieved $b_p(440)$ values are always lower than 6% and are 0.30% on average. Moreover, the correction proposed is valid independently of the near-IR slope γ value (Fig. 12C). Note that Eq. 12 was derived from theoretical calculations, independently from our in situ data set. Moreover, Eq. 12 is expected to apply at any visible wavelength (here 440, 555, and 630 nm were considered in computations) even if it was only validated by field measurements at 440 nm.

Discussion

A simple power-law function (Eq. 9) closely reproduced the near-IR spectral variations of the scattering coefficient of marine particles of coastal origin. This assumption, already verified in turbid estuarine waters (Doxaran et al. 2007), was confirmed here for a wide range of coastal waters. On the basis of available field observations, typical values for the particulate scattering spectral slope in the near IR were: (1) 0.4 ± 0.3 in highly turbid estuarine waters

($b_p[715] > 10 \text{ m}^{-1}$), (2) 0.6 ± 0.5 in moderately turbid waters ($1 < b_p[715] < 10 \text{ m}^{-1}$), and (3) 0.8 ± 0.3 in less turbid waters ($b_p[715] < 1 \text{ m}^{-1}$). This near-IR spectral slope clearly increased from 0.1 to 1.4 as the water turbidity decreased. Its variations were most probably related to changes in the PSD.

On the basis of field measurements, the relationship between the visible and near-IR spectral slopes of the particulate scattering coefficient is linear with a slope close to 1 but a significant intercept of -0.0923 (Fig. 8), provided that wave bands associated with strong particulate absorption are avoided (e.g., 440 nm). In the visible part of the spectrum, particulate absorption effects on scattering properties are systematically significant. In the coastal waters sampled, differences of 10% on average and up to 35% were observed at 440 nm between actual b_p values and b_p values modeled using a power-law function fitted on the near-IR wave bands and extrapolated to 440 nm. On the basis of theory and under several simplifying assumptions, the departure of $b_p(\lambda)$ from a power-law function (Eq. 9) is almost equal to the particulate absorption coefficient (a_p) when the particle size distribution presents a high proportion of coarse particles (e.g., particles following a Junge size distribution with an exponent $j \leq 3.4$). The decrease of $b_p(\lambda)$ due to particulate absorption effects becomes a complex function of a_p , the particle size distribution and real part of the refractive index, when the proportion of small particles increases (e.g., particles following a Junge size distribution with an exponent $j \geq 3.6$). Small particles are less efficient than coarse ones in terms of light absorption, so that light scattering by submicrometric particles is little affected by particulate absorption. On the basis of Mie scattering calculations, an empirical formulation (Eq. 12) has been established to model the particulate absorption effect on particulate scattering, taking into account the particle size distribution and $a_p(\lambda)$. It was confirmed on the basis of numerous field measurements carried out in various coastal waters. The in situ instrumentation used in our study, with several discrete bands, is not an ideal approach to experimentally address the question of spectral slope of scattering. Ultimately, accurate hyperspectral measurements of both the scattering and absorption from various environments will be needed to fully validate our results. This study allows us to propose a new model to express realistic spectral variations in $b_p(\lambda)$ from the near-IR to the visible spectral domains:

$$b_p(\lambda) = b_p(\lambda_{\text{ref}}) \times \left(\frac{\lambda}{\lambda_{\text{ref}}} \right)^{-\gamma} - [1 - \tanh(0.5 \times \gamma^2)] \times a_p(\lambda) \quad (13)$$

with λ_{ref} a reference wavelength and γ the spectral slope of b_p , both in a spectral domain where particulate absorption is almost negligible, i.e., the near IR.

This b_p scattering model accurately corrects for particulate absorption effects when marine particles follow a Junge size distribution and reproduced field measured $b_p(\lambda)$ with an error lower than 6%. It should be used to express in a more realistic way the spectral variations of the particle scattering

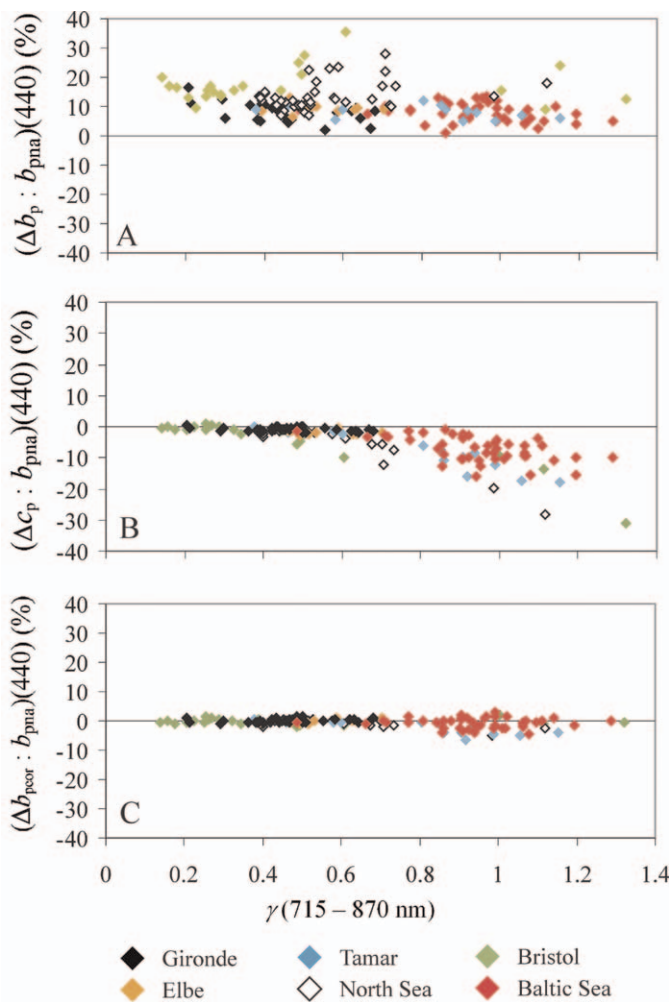


Fig. 12. Plot of the measured (A) $(\Delta b_p : b_{pna})(440)$, (B) $(\Delta c_p : b_{pna})(440)$, and (C) $(\Delta b_{pcorr} : b_{pna})(440)$ differences, in percentage, as a function of the b_p (715–870 nm) spectral slope.

coefficient when modeling the inherent optical properties of seawater. As a first application, it may be included into radiative transfer codes, such as the widely used HYDRO-LIGHT (Sequoia Scientific), which compute the propagation of light with natural waters. The potential application to ocean color remote sensing, e.g., in the Garver–Siegel–Maritorena (Maritorena et al. 2002) and Doerffer and Schiller (2007) algorithms, will require further investigation to determine how the spectral variations of light backscattering by hydrosols is affected by particulate absorption.

Acknowledgments

We are very grateful to the scientists of different institutions who provided their support during the field campaigns. We notably thank J. Seppälä and S. Simis from the Finnish Institute of Marine Research, who gave us access to the RV *Aranda* for a cruise in the Baltic Sea. Two anonymous reviewers and the associate editor are acknowledged for their careful reading of the original paper and helpful suggestions. This paper is dedicated to the memory of Dominique Tailliez.

This study was funded by a European Reintegration Grant (contract ERG-14905 RSFLUX), the Centre National d'Etudes

Spatiales (CNES-France), and the BELCOLOUR-2 project (funded by the Belgian Science Policy Office STEREO-2 programme).

References

- AAS, E. 1996. Refractive index of phytoplankton derived from its metabolite composition. *J. Plankton Res.* **18**: 2223–2249.
- AGRAWAL, Y. C., AND H. C. POTTS. 2000. Instruments for particle size and settling velocity in sediment transport. *Mar. Geol.* **168**: 89–114.
- BABIN, M., A. MOREL, V. FOURNIER-SICRE, F. FELL, AND D. STRAMSKI. 2003a. Light scattering properties of marine particles in coastal and oceanic waters as related to the particle mass concentration. *Limnol. Oceanogr.* **48**: 843–859.
- , AND D. STRAMSKI. 2002. Light absorption by aquatic particles in the near-infrared spectral region. *Limnol. Oceanogr.* **47**: 911–915.
- , AND ———. 2004. Variations in the mass-specific absorption coefficient of mineral particles suspended in water. *Limnol. Oceanogr.* **49**: 756–767.
- , ———, G. M. FERRARI, H. CLAUSTRE, A. BRICAUD, G. OBOLENSKY, AND N. HOEPFFNER. 2003b. Variations in the light absorption coefficients of phytoplankton, nonalgal particles, and dissolved organic matter in coastal waters around Europe. *J. Geophys. Res.* **108**: 3211–3230.
- BADER, H. 1970. The hyperbolic distribution of particle sizes. *J. Geophys. Res.* **75**: 2822–2830.
- BALE, A. J., AND A. W. MORRIS. 1987. In situ measurements of particle size in estuarine waters. *Estuar. Coast. Shelf Sci.* **24**: 253–263.
- BARNARD, A. H., W. S. PEGAU, AND J. R. V. ZANEVELD. 1998. Global relationships of the inherent optical properties of the oceans. *J. Geophys. Res.* **75**: 2837–2845.
- BERNARD, S., T. A. PROBYN, AND R. G. BARLOW. 2001. Measured and modeled optical properties of particulate matter in the southern Benguela. *S. Afr. J. Sci.* **97**: 410–420.
- BOHREN, C. F., AND D. F. HUFFMANN. 1983. Absorption and scattering of light by small particles. Wiley.
- BOSS, E., M. S. TWARDOWSKI, AND S. HERRING. 2001b. Shape of the particulate beam attenuation spectrum and its inversion to obtain the shape of the particulate size distribution. *Appl. Opt.* **40**: 4885–4893.
- , AND OTHERS. 2001a. Spectral particulate and particle size distribution in the bottom boundary layer of a continental shelf. *J. Geophys. Res.* **106**: 9509–9516.
- BRICAUD, A., A. L. BEDHOMME, AND A. MOREL. 1988. Optical properties of diverse phytoplanktonic species: Experimental results and theoretical interpretation. *J. Plankton Res.* **10**: 851–873.
- , AND A. MOREL. 1986. Light attenuation and scattering by phytoplanktonic cells: A theoretical modelling. *Appl. Opt.* **25**: 571–580.
- CHAMI, M., E. B. SHYBANOV, G. KHOMENKO, M. LEE, O. V. MARTYNOV, AND G. KOROTAEV. 2006. Spectral variation of the volume scattering function measured over the full range of scattering angles in a coastal environment. *Appl. Opt.* **45**: 3605–3619.
- DALL'OLMO, G., AND A. A. GITELSON. 2005. Effect of bio-optical parameter variability on the remote estimation of chlorophyll-a concentration in turbid productive waters: Experimental results. *Appl. Opt.* **44**: 412–422.
- DOERFFER, R., AND H. SCHILLER. 2007. The MERIS case 2 water algorithm. *Int. J. Remote Sens.* **28**: 517–535.
- DOXARAN, D., M. BABIN, AND E. LEYMARIE. 2007. Near-infrared light scattering by particles in coastal waters. *Opt. Express.* **15**: 12834–12849.

- , J. M. FROIDEFOND, S. J. LAVENDER, AND P. CASTAING. 2002. Spectral signature of highly turbid waters. Application with SPOT data to quantify suspended particulate matter concentrations. *Remote Sens. Environ.* **81**: 149–161.
- ECK, T., B. N. HOLBEN, O. DUBOVIK, A. SMIRNOV, N. O'NEILL, I. SLUTSKER, AND S. KINNE. 1999. Wavelength dependence of the optical depth of biomass burning, urban and desert dust aerosols. *J. Geophys. Res.* **104**: 31333–31349.
- EGAN, W. G., AND T. W. HILGEMAN. 1979. Optical properties of inhomogeneous materials: Applications to geology, astronomy, chemistry, and engineering. Academic.
- EISMA, D., AND OTHERS. 1991. Suspended-matter particle size in some West-European estuaries; Part I: Particle-size distribution. *Neth. J. Sea Res.* **28**: 193–214.
- JONASZ, M., AND G. FOURNIER. 2007. Light scattering by particles in water. Theoretical and experimental foundations. Academic Press, Elsevier.
- KRANCK, K. 1984. The role of flocculation in the filtering of particulate matter in estuaries. In V. S. Kennedy [ed.], *The estuary as a filter*. Academic Press.
- LANGFORD, V. S., A. J. MCKINLEY, AND T. I. QUICKENDEN. 2001. Temperature dependence of the visible–near-infrared absorption spectrum of liquid water. *J. Phys. Chem. A* **105**: 8916–8921.
- LEE, Z. P., K. P. DU, AND R. ARNONE. 2005. A model for the diffuse attenuation coefficient of downwelling irradiance. *J. Geophys. Res.* **110**: C02016, doi:10.1029/2004JC002275.
- LIDE, D. R. 2001. *Handbook of physics and chemistry*, 82nd ed. CRC.
- MARITORENA, S., D. A. SIEGEL, AND A. PETERSON. 2002. Optimization of a semianalytical ocean color model for global-scale applications. *Appl. Opt.* **41**: 2705–2714.
- MCKEE, D., AND A. CUNNINGHAM. 2006. Identification and characterisation of two optical water types in the Irish Sea from in situ inherent optical properties and seawater constituents. *Estuar. Coast. Shelf Sci.* **68**: 305–316.
- MOORE, G. F., J. AIKEN, AND S. J. LAVENDER. 1999. The atmospheric correction of water colour and the quantitative retrieval of suspended particulate matter in case II waters: Application to MERIS. *Int. J. Remote Sens.* **20**: 1713–1733.
- MOREL, A. 1973. Light scattering by seawater. Experimental results and theoretical approach, p. 3.1.1–3.1.76. In *Optics of the sea*. AGARD Lect. Ser., NATO, Neuilly-sur-Seine. (Diffusion de la lumière par les eaux de mer. Résultats expérimentaux et approche théorique.)
- , AND Y. H. AHN. 1990. Optical efficiency factors of free-living marine bacteria: Influence of bacterioplankton upon the optical properties and particulate organic carbon in oceanic waters. *J. Mar. Res.* **48**: 145–175.
- , AND A. BRICAUD. 1981. Theoretical results concerning the optics of phytoplankton, with special references to remote sensing applications, p. 313–327. In J. F. R. Gower [ed.], *Oceanography from space*. Plenum.
- , AND ———. 1986. Inherent optical properties of algal cells, including picoplankton. Theoretical and experimental results. *Canadian Bull. Fish. Aquatic Sci.* **214**: 521–559.
- , AND S. MARITORENA. 2001. Bio-optical properties of oceanic waters: A reappraisal. *J. Geophys. Res.* **106**: 7763–7780.
- PATTERSON, E. M., D. A. GILLETTE, AND B. H. STOCKTON. 1977. Complex index of refraction between 300 and 700 nm for Saharan aerosols. *J. Geophys. Res.* **82**: 3153–3160.
- PEGAU, W. S., D. GRAY, AND J. R. V. ZANEVELD. 1997. Absorption and attenuation of visible and near-infrared light in water: Dependence on temperature and salinity. *Appl. Opt.* **36**: 6035–6046.
- PISKOZUB, J., D. STRAMSKI, E. TERRIL, AND W. K. MELVILLE. 2004. Influence of forward and multiple light scatter on the measurements of beam attenuation in highly scattering marine environments. *Appl. Opt.* **43**: 4723–4731.
- RISOVIC, D. 2002. Effect of suspended particulate-size distribution on the backscattering ratio in remote sensing of seawater. *Appl. Opt.* **41**: 7092–7101.
- ROESLER, C. S., AND M. J. PERRY. 1995. In situ phytoplankton absorption, fluorescence emission, and particulate backscattering spectra determined from reflectance. *J. Geophys. Res.* **100**: 13279–13294.
- RUDDICK, K. G., V. DE CAUWER, Y. J. PARK, AND G. F. MOORE. 2006. Seaborne measurements of near infrared water-leaving reflectance: The similarity spectrum for turbid waters. *Limnol. Oceanogr.* **51**: 1167–1179.
- SATHYENDRANATH, S., L. PRIEUR, AND A. MOREL. 1989. A three-component model of ocean colour and its application to remote sensing of phytoplankton pigments in coastal waters. *Int. J. Remote Sens.* **10**: 1373–1394.
- SNYDER, W. A., AND OTHERS. 2008. Optical scattering and backscattering by organic and inorganic particulates in U.S. coastal waters. *Appl. Opt.* **47**: 666–677.
- STAVN, R. H., AND T. R. KEEN. 2004. Suspended minerogenic particle distributions in high-energy coastal environments: Optical implications. *J. Geophys. Res.* **109**, doi:10.1029/2003JC002098.
- STRAMSKI, D., M. BABIN, AND S. B. WOŹNIAK. 2007. Variations in the optical properties of terrigenous mineral-rich particulate matter suspended in seawater. *Limnol. Oceanogr.* **52**: 2418–2433.
- , A. BRICAUD, AND A. MOREL. 2001. Modeling the inherent optical properties of the ocean based on the detailed composition of the planktonic community. *Appl. Opt.* **40**: 2929–2945.
- , AND S. B. WOŹNIAK. 2005. On the role of colloidal particles in light scattering in the ocean. *Limnol. Oceanogr.* **50**: 1581–1591.
- , ———, AND P. J. FLATAU. 2004. Optical properties of Asian mineral dust suspended in seawater. *Limnol. Oceanogr.* **49**: 749–755.
- SULLIVAN, J. M., M. S. TWARDOWSKI, J. R. V. ZANEVELD, C. M. MOORE, A. H. BARNARD, P. L. DONAGHAY, AND B. RHOADES. 2006. Hyperspectral temperature and salt dependence of absorption by water and heavy water in the 450–750-nm spectral range. *Appl. Opt.* **45**: 5294–5309.
- VAN DER LINDE, D. W. 1998. Protocol for determination of total suspended matter in oceans and coastal zones. JRC Tech. Note.
- WOŹNIAK, S. B., AND D. STRAMSKI. 2004. Modeling the optical properties of mineral particles suspended in seawater and their influence on ocean reflectance and chlorophyll estimation from remote sensing algorithms. *Appl. Opt.* **43**: 3489–3503.
- ZANEVELD, J. R. V., J. C. KITCHEN, AND C. C. MOORE. 1994. Scattering error correction of reflecting tube absorption meters. *Proc. SPIE* **2258**: 44–55.

Associate editor: Dariusz Stramski

Received: 20 June 2008

Accepted: 27 February 2009

Amended: 05 March 2009